HHS Public Access

Author manuscript

ACS Appl Bio Mater. Author manuscript; available in PMC 2019 December 17.

Published in final edited form as:

ACS Appl Bio Mater. 2018 December 17; 1(6): 1918–1926. doi:10.1021/acsabm.8b00488.

Water-Dispersible Bismuth–Organic Materials with Computed Tomography Contrast Properties

Guoxian Zhang[†], **Pratap C. Naha**[‡], **Prabhat Gautam**[†], **David P. Cormode**[‡], **Julian M. W. Chan**[*,†]

[†]Department of Chemistry and Biomolecular Sciences, University of Ottawa, 10 Marie Curie Pvt., Ottawa, Ontario K1N 6N5, Canada

[‡]Department of Radiology, University of Pennsylvania, Philadelphia, Pennsylvania 19104, United States

Abstract

Two bismuth–organic network polymers were synthesized by means of a one-step polycondensation reaction between an aromatic dithiol/trithiol and triphenylbismuth. The materials were characterized by solid-state UV–vis spectroscopy, Raman spectroscopy, scanning electron microscopy, energy dispersive X-ray spectroscopy, powder X-ray diffraction, elemental microanalysis, and thermogravimetric analysis. Uniform dispersion of the hydrophobic and water-insoluble bismuth-containing polymers in aqueous media was achieved by the addition of 2 kDa poly(ethylene glycol) methyl ether thiol. This enabled quantitative phantom imaging experiments on a clinical computed tomography (CT) scanner, which showed that the coordination polymers possessed strong CT contrast properties. The observed X-ray attenuation properties of each coordination polymer were correlated with its bismuth payload. The X-ray opacity, thermal and chemical stabilities, and aqueous dispersibility of this novel class of bismuth–organic materials make them potentially useful as biomedical CT contrast agents and radiopaque materials.

Graphical Abstract

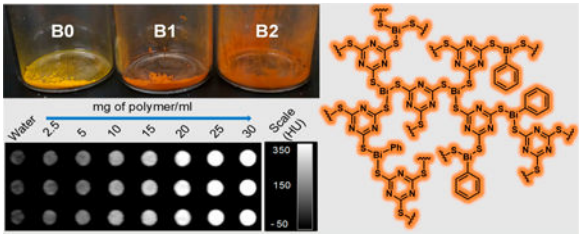

Keywords

CT contrast agents; X-ray contrast; bismuth thiolates; coordination polymers; organic–inorganic hybrid materials; radiopaque polymers

[*]Corresponding Author julian.chan@uottawa.ca.

The authors declare no competing financial interest.

INTRODUCTION

Radiopaque materials, such as synthetic polymers that possess X-ray contrast properties, have attracted significant interest due to their practical utility in the field of biomedical imaging. For example, radiopaque polymers[1–7] have been employed in dental plastics, implantable medical devices, for example, stents,[8] catethers,[9] or fiducial markers used to delineate regions of interest within the human body,[10] and nanoscale computed tomography (CT) contrast agents[11,12] for noninvasive imaging. Beyond the medical field, radiopaque polymers have also recently been used as photoresists in two-photon lithography, whereby submicron three-dimensional (3D) imaging was achieved using X-ray CT.[13]

In the context of dental materials and implantable devices, early methods for imparting radiopacity to a material often involved blending heavy metal salts such as barium sulfate (Ba, atomic number $Z = 56$) with an organic polymer.[14,15] This was nonideal due to the incompatibility between the polymer matrix and the inorganic salts, which often lead to heterogeneity, compromised mechanical properties, and reduced aesthetic properties of the final resin.[16] Furthermore, despite the low solubility of $BaSO_4$, it has been suspected that the heavy metal salt may be harmful or even bioaccumulate in the body.[17] An alternative approach has been to use halogenated polymers containing heavy atoms such as Br ($Z = 35$) or I ($Z = 53$), but these tend to have diminished stability on prolonged contact with biological milieu and/or light.[18] Similarly, styrenic polymers containing bismuth (Z = 83) on diphenylbismuth-functionalized pendant side chains have also be synthesized and shown to have good radiopacity,[19] though the maximum attainable Bi content in those polymers was just under 45%. Another potential limitation stems from the fact that Bi–C bonds are pH-sensitive, which would likely preclude any applications that involve in vivo biological imaging.

As for low-toxicity nanoscale CT contrast agents, research in this area has grown exponentially in recent years. This interest is driven by the ability of these materials to evade renal clearance, leading to longer circulation times that offer the possibility of blood pool and site-directed CT imaging.[20–25] Here as well, compounds containing heavy elements are effective in producing CT contrast due to their X-ray opacity. Iodinated organic molecules such as Iopamidol and Iohexol are used clinically as CT contrast agents, though there have been concerns about their biocompatibility, particularly in individuals with impaired renal function.[26,27] Consequently, alternative CT contrast agents based on gold[28–32] (Z = 79) and bismuth[33–45] (Z = 83) have been explored in recent years. Compared to iodinated agents, Au- and Bi-based materials possess higher X-ray opacity due to their higher atomic numbers, and they also exhibit low toxicity and excellent biocompatibility.[46–48] Between Au- and Bi-based agents, each comes with a unique combination of advantages and drawbacks. With Au, the wealth of literature on Au nanoparticle (NP) preparation and the oxidative inertness of Au are advantageous for synthesis and formulation.[49–51] That same inertness, however, does pose a risk of bioaccumulation and long-term toxicity.[52] In comparison, Bi is much less expensive per mole than Au, has a similar level of nontoxicity and biocompatibility, and can slowly oxidize and hydrolyze to renally clearable Bi(III) species.[53] The challenges associated with Bi contrast agents are mainly synthetic, that is, the methodologies for synthesis are less developed than those of Au NPs, and the hydrolytic

instability of BiNPs,[54] while 83 advantageous for nonbioaccumulation, poses problems for aqueous synthesis.

With its low cost and low toxicity, bismuth is an attractive element for radiopaque materials and CT contrast agents. Herein, we report two novel bismuth thiolate network coordination polymers **B1** and **B2** (Figure 1) that exhibit strong CT contrast properties and water-dispersibility. These materials contain Bi in the +3 oxidation state, where Bi(III) nodes are connected by tritopic aromatic thiol linkers. Previously, we reported a related class of thermochromic bismuth–organic materials featuring Bi(III) nodes that were doubly rather than triply connected to dithiol linkers,[55] exemplified by the reference material **B0**. On the one hand, these earlier materials were synthesized by polycondensations between triphenylbismuth and dithiols in refluxing toluene, giving structures that were more linear in nature and with limited Bi content (<50%). The new materials **B1** and **B2**, on the other hand, were synthesized by reacting triphenylbismuth with a trithiol, which afforded structures of higher Bi content, a key factor for achieving desirable X-ray contrast.

RESULTS AND DISCUSSION

Molecular Design and Synthesis.

The coordination polymer **B0** was previously reported by our group as part of an unrelated study on thermochromic organic–inorganic materials.[55] In the present study, **B0** is used a s a reference against which the novel materials **B1** and **B2** were compared. As previously published, **B0** was synthesized by refluxing triphenylbismuth with benzene-1,4-dithiol in toluene over 3 d. The reaction, as well as related ones, is believed to proceed via thermally initiated radical-based pathways.[56–61] When performed in refluxing toluene (bp 110 °C), the reaction resulted in the substitution of two phenyl moieties on Ph_3Bi by sulfur, even when excess equivalents of thiol were used. This propensity for double substitution gives polymers featuring repeat units of limited Bi content. Early studies by Gilman et al. revealed that higher levels of substitution could be achieved by performing the same reaction in refluxing xylene (bp 140 °C),[62] suggesting that the Bi centers became less reactive with each substitution and required higher temperatures for further substitution.

Within the context of X-ray contrast materials, our key objective was to maximize the heavy element payload. In the case of **B0**, the bismuth content was only 49% by mass. The molecular design of structures **B1**/**B2** was aimed at boosting the bismuth payload beyond 49%. More precisely, by replacing the ditopic dithiol linker in **B0** with a trithiol, repeat units with higher percentage Bi would result. Additionally, by performing the polycondensation at xylene reflux temperatures, triple versus double substitution around Bi could be favored to afford a network structure with enhanced Bi content. Compared with **B0**, which has an undesirably high light-element (C, H, N, S) content of 51%, microanalysis indicated that the CHNS contents of **B1** and **B2** were 45.9% and 41.1%, respectively. This was later correlated with the X-ray attenuation ability of each material in CT experiments (cf. section on phantom CT imaging). Our motivation for the use of *s*-triazine-based organic linkers in place of benzene-based connectors was twofold. The first idea was to facilitate dispersion of the material in aqueous media via H bonding between the heterocycle nitrogens and H_2O

molecules (though this was subsequently found to be immaterial). Second, 1,3,5-triazine-2,4,6-trithiol, or trithiocyanuric acid, is much less costly than arene-1,4-dithiols and benzene-1,3,5-trithiol, making it an ideal tritopic molecular building block for affordable functional materials. Both materials **B1** and **B2** were readily synthesized through facile one-step polycondensations between trithiocyanuric acid and triphenylbismuth in refluxing toluene and xylene, respectively (Scheme 1). The sole byproduct of the reaction was benzene, which was easily removed along with the reaction solvents by suction filtration and subsequent drying under high vacuum.

UV–Vis and Raman Spectroscopy.

Materials **B1** and **B2** were isolated as insoluble orange solids. Spectroscopic characterization of **B1** and **B2** by solid-state UV–vis diffuse reflectance spectroscopy showed absorption profiles with band edges at 580 and 610 nm, respectively (Figure 2). corresponding optical band gaps as calculated by the Tauc plot method are 2.15 and 2.03 eV, respectively. The observed absorption features between 350–450 nm were consistent with S → Bi ligand-to-metal charge-transfer (LMCT) bands.[63–65] The optical gaps were narrower than that of the reference material **B0** (E_g = 2.28 eV), which was consistent with higher degrees of sulfur substitution around the bismuth nodes. Between **B1** and **B2**, the slightly narrower optical bandgap of the latter suggests a greater extent of triply substituted bismuth, as would be expected from a reaction conducted in the higher-boiling solvent.

Additionally, Raman spectroscopy was also performed on the two amorphous materials. Within the Raman spectra of **B1** and **B2** were shoulder features that can be observed around 230–240 cm^{-1} (Figure 3), overlapping with the lattice vibration region (100–200 cm^{-1}). These are characteristic low-frequency bands that can be attributed to Bi–S bond vibrations. Raman bands arising from Bi–S are typically observed in the 185–260 cm^{-1} region, as in the case of the well-studied bismuth sulfide systems.[66–68] The minor feature at 970–980 cm^{-1}, which is often associated with bismuth–sulfur systems, is attributed to Bi–O formed by laser-induced photo-oxidation.[66] The features between 1200 and 1700 cm^{-1}, such as the *D*- and *G*-bands at the characteristic shifts of 1350 and 1600 cm^{-1}, are typical of aromatic materials containing sp^2-hybridized carbons.

Scanning Electron Microscopy/Energy-Dispersive X-ray Spectroscopy.

To supplement the spectroscopic studies described above, the two new bismuth thiolate coordination polymers **B1** and **B2** were also characterized by scanning electron microscopy (SEM)/energy-dispersive X-ray spectrosopy (EDS). The SEM images of both materials revealed morphologies that suggested an amorphous nature (Figure 4), in contrast to **B0**, which exhibits rodlike crystallites at the microscale level.[55] The amorphous nature of **B1** and **B2** was further confirmed by powder X-ray diffraction (PXRD) studies, which indicated the absence of long-range ordering (Figure 4). EDS was performed in conjunction with the SEM studies to complement our CHNS analysis results. The EDS data confirmed the elemental compositions of the two materials, with C, Bi, and S producing the most prominent signals (Figure 5).

Thermogravimetric Analysis.

The thermal stabilities of **B1** and **B2** in air were evaluated using thermogravimetric analysis (TGA). The materials were heated in air using a heating rate of 10 °C per minute, and both were found to possess excellent stability up to ~300 °C, before significant weight loss occurred (Figure 6). Some of the initial minor decreases in weight at lower temperatures can be attributed to adsorbed or trapped water molecules, and in the case of **B2**, traces of xylene being thermally driven off. Overall, the temperatures corresponding to a 5% weight loss were 307 and 265 °C for **B1** and **B2**, respectively, while major decomposition was only observed to occur above 300 °C.

Phantom CT Imaging.

The X-ray contrast properties of **B0, B1**, and **B2** were studied using a clinical CT scanner. The CT phantom was prepared according to a previously reported protocol.[69] Briefly, three separate stock solutions were prepared by suspending each bismuth-thiolate polymer (50 mg) in deionized water (1 mL) containing 80 mg of 2 kDa poly(ethylene glycol) methyl ether thiol (i.e., m-PEG-SH). The use of the hydrophilic m-PEG-SH was found to be necessary for achieving uniform dispersion of the water-insoluble materials. This was expected, given that thiol groups exhibit strong affinity for soft metals such as bismuth. From the three stock solutions, polymer samples with concentrations ranging from 2.5 to 30 mg/mL were made in 1% agarose gel in 200 μL Eppendorf tubes. The samples were then scanned on the clinical CT scanner at four commonly employed X-ray tube voltages 80, 100, 120, and 140 kV (see Experimental Section for details). A set of examples showing three CT images obtained for **B0, B1**, and **B2** scanned at 80 kV is depicted in Figure 7. The CT attenuation value in Hounsfield units (HU) for each sample tube was recorded from three different slices and averaged for each concentration. The data are presented as average CT attenuation values in HU and error bars represent the standard deviations (n = 3). Compared to the reference material B0, which had the lowest percentage bismuth by mass, **B1** and **B2** displayed stronger X-ray attenuation consistent with higher heavy atom content. On the one hand, attenuation was strongest at 80 kV, with HU values that were 10–20% higher than at other X-ray tube voltages. On the other hand, attenuation values were relatively constant between 100 and 140 kV, similar to patterns observed with previously reported Bi NPs.[34] This is most probably due to the high k-edge of Bi (90.8 keV) compared to the average energy of the X-ray beam employed in the specific CT scanner. We compared the contrast production of the polymers with that of Iopamidol, a Food and Drug Administration (FDA)-approved iodine-based X-ray contrast agent (Figure 7d). To do this comparison, we normalized the concentrations in terms of the molarity of the contrast-generating atoms of the different agents. As can be seen, when this normalization is done, **B0, B1**, and **B2** all produce very similar contrast, as expected. Iopamidol produces less contrast than the bismuth-based agents at each tube voltage used, and its contrast production reduces as the tube voltage increases. These results are in line with previous reports.[35] These data support the potential value of these bismuth thiolate polymers, since their contrast performance exceeds that of the clinically used agent.

A limitation of this study is that the in vivo safety of these polymers was not assessed. This is a key question for biomaterials and will be the subject of future work. Nevertheless, we

expect that these polymers would have a good safety profile for several reasons, based on the premise that their likely decomposition products would be Bi(III) and trithiocyanuric acid. First, bismuth is regarded as being one of the safest heavy elements. For example, administration of 140 mg/d of Bi^{3+} has been found to be safe in clinical trials.[70] Second, the other component of the polymer, trithiocyanuric acid, has an extremely high LD_{50} of 9.5 g/kg (see material safety data sheet (MSDS) of trithiocyanuric acid via www.sigmaaldrich.com), which supports the safety of this component. Nevertheless, safety testing of these polymers will be needed, as for any novel material.

EXPERIMENTAL SECTION

Materials and Methods.

Chemical synthesis was performed using oven-dried glassware under dry N_2 by means of standard Schlenk techniques. The necessary chemicals/reagents and solvents were obtained from Sigma-Aldrich and Fisher Scientific and employed without additional purification. Water traces were removed from organic solvents using activated 3 Å molecular sieves, and the solvents were also degassed thoroughly by purging with nitrogen gas before use. UV–Vis diffuse reflectance spectra (DRS) of the powdered products were recorded as previously reported.[55] PXRD analyses were done on a Rigaku Ultima IV diffractometer housed in the University of Ottawa X-ray Core Facility. SEM/EDS analysis was performed using a JSM-7500 FESEM (JEOL) instrument. Raman spectroscopy was performed on a Horiba Xplora Plus confocal Raman microscope. The Raman spectra were collected using ×100 optics with a 532 nm laser at 25% of full power (17.5 μW). Elemental microanalysis (CHNS) was performed by the University of Alberta Analytical and Instrumentation Laboratory. The TGA results were acquired using a TGA Q500 (TA Instruments) at the Center for Self-Assembled Chemical Structures (CSACS) at McGill University, where the samples were heated in air from 25 to 500 °C using a heating rate of 10 °C/min, and the data were analyzed on the TA Instruments Universal Analysis 2000 Version 4.5 A.

Synthesis of Triphenylbismuth (1).

Ph_3Bi was synthesized and purified according to previously published procedures[55] and subsequently used for the preparation of **B1** and **B2.**

Synthesis of B1.

A solution of 1,3,5-triazine-2,4,6-trithiol (0.177 g, 1.00 mmol) in tetrahydrofuran (THF; 5 mL) was added to a refluxing solution of triphenylbismuth (0.440 g, 1.00 mmol) in anhydrous degassed toluene (70 mL). This mixture was subjected to vigorous stirring over a period of 72 h, during which an orange precipitate was formed. After the completion of the reaction, the solution was allowed to slowly cool to room temperature. The orange precipitate was then filtered off, washed several times with acetone, and finally placed under high vacuum at 120 °C for 24 h to obtain the final product **B1** as a dry orange powder. Yield: 0.273 g, 71.3%. Anal. Calcd for $(C_3BiN_3S_3)_{0.85}(C_9H_6BiN_3S_3)_{0.15}\cdot 0.8\ H_2O$ (formula of one repeat unit): C, 11.44; H, 0.62; N, 10.27; S, 23.50. Found: C, 11.44; H, 0.57; N, 10.07; S, 23.77%.

Synthesis of B2.

A solution of 1,3,5-triazine-2,4,6-trithiol (0.177 g, 1.00 mmol) in THF (5 mL) was added to a refluxing solution of triphenylbismuth (0.440 g, 1.00 mmol) in anhydrous degassed xylene (70 mL). This mixture was then stirred vigorously over a period of 72 h, during which an orange precipitate was formed. Upon conclusion of the reaction, the solution was allowed to gradually cool to room temperature, whereupon the orange solid was filtered, washed with acetone, and then placed under high vacuum at 120 °C to dry over 24 h. Yield: 0.231 g, 60.3%. Anal. Calcd for the formula of the repeat unit $(C_3BiN_3S_3)\cdot 3.5\ H_2O\cdot 0.2\ C_8H_{10}$ (xylene): C, 11.82; H, 1.94; N, 8.99; S, 20.57. Found: C, 11.51; H, 0.64; N, 8.59; S, 20.40%.

Phantom CT Imaging.

Bismuth thiolate polymer (i.e., **B0, B1**, and **B2**) and Iopamidol (ISOVUE-300, Bracco Diagnostics) phantom was prepared and scanned with a clinical CT scanner according to a previously described protocol.[69] The bismuth-based polymers (50 mg each) were suspended in deionized water (1 mL) containing 80 mg of 2 kDa m-PEG-SH (Creative PEGWorks). From this stock solution, a range of polymer concentrations, that is, 2.5, 5, 10, 15, 20, 25, and 30 mg/mL, were made in 1% agarose gel in 200 μL Eppendorf tubes. Iopamidol was diluted to 0.5, 1, 2, 4, 6, 8, and 10 mg/mL in deionized water. Next, the tubes were positioned within a plastic rack and wrapped with parafilm. This rack was subsequently placed in a plastic container containing water up to a height of 21 cm to simulate the attenuation effects in a patient. The phantom was scanned on a Siemens SOMATOM Force 192-slice clinical CT scanner at the following tube voltages: 80, 100, 120, and 140 kV. The matrix size and slice thickness used were 512 × 512 and 0.5 mm, respectively. The tube current used was 360 mA for each voltage, and convolution kernel Br 40d was used. Osirix MD 64-bit software was used for analyzing the CT images. The CT attenuation value in HU for each sample tube was recorded from three different slices and averaged for each concentration. The data are given as average CT attenuation values in HU, and the error bars represent the standard deviations ($n = 3$).

CONCLUSIONS

In summary, we report a bismuth thiolate coordination polymer system that was synthesized via a facile polycondensation between triphenylbismuth and a heterocyclic trithiol. The percentage bismuth content of the materials could be controlled by manipulating the reaction temperatures at which the reaction is performed. The pair of novel bismuth–organic materials was characterized by solid-state UV–vis spectroscopy, Raman spectroscopy, PXRD, SEM, EDS, elemental analysis, and TGA. Both materials were found to be thermally stable and dispersible in water upon coaddition of a thiol-terminated 2 kDa PEG. This dispersibility allowed for systematic dilution and subsequent phantom CT imaging experiments on a clinical CT scanner. The imaging experiments showed that the polymers possessed strong X-ray contrast properties that could be correlated with their percentage bismuth content. In this way, the X-ray attenuation abilities of the coordination polymers can be indirectly controlled by the choice of reaction conditions under which the materials are synthesized. The coordination polymers described herein may be of interest and utility as

radiopaque materials for medical devices, biomaterials, and/or X-ray contrast agents for imaging.

ACKNOWLEDGMENTS

This research was funded by a Discovery Grant (RGPIN-2016-04614) from the Natural Sciences and Engineering Research Council, a John R. Evans Leaders Fund from the Canada Foundation for Innovation (Project No. 34474), the Ministry of Research and Innovation in Ontario, and the Univ. of Ottawa. D.P.C. thanks the National Institutes of Health for funding (R01-HL131557).

REFERENCES

(1). Goodfriend AC; Welch TR; Nguyen KT; Wang J; Johnson RF; Nugent A; Forbess JM Poly(gadodiamide fumaric acid): A Bioresorbable, Radiopaque, and MRI-Visible Polymer for Biomedical Applications. ACS Biomater. Sci. Eng 2015, 1, 677–684.

(2). Kiran S; James NR; Joseph R; Jayakrishnan A Synthesis and Characterization of Iodinated Polyurethane with Inherent Radiopacity. Biomaterials 2009, 30, 5552–5559. [PubMed: 19596151]

(3). Górecka Ż; Teichmann J; Nitschke M; Chlanda A; Choińska E; Werner C; Święszkowski W Biodegradable Fiducial Markers for X-ray Imaging-Soft Tissue Integration and Biocompatibility. J. Mater. Chem. B 2016, 4, 5700–5712.

(4). Samuel R; Girard E; Chagnon G; Dejean S; Favier D; Coudane J; Nottelet B Radiopaque Poly(3-caprolactone) as Additive for X-ray Imaging of Temporary Implantable Medical Devices. RSC Adv 2015, 5, 84125–84133.

(5). Ma Q; Lei K; Ding J; Yu L; Ding J Design, Synthesis and Ring-opening Polymerization of a New Iodinated Carbonate Monomer: A Universal Route towards Ultrahigh Radiopaque Aliphatic Polycarbonates. Polym. Chem 2017, 8, 6665–6674.

(6). deKrafft KE; Xie Z; Cao G; Tran S; Ma L; Zhou OZ; Lin W Iodinated Nanoscale Coordination Polymers as Potential Contrast Agents for Computed Tomography. Angew. Chem., Int. Ed 2009, 48, 9901–9904.

(7). Ghosh P; Das M; Rameshbabu AP; Das D; Datta S; Pal S; Panda AB; Dhara S Chitosan Derivatives Cross-Linked with Iodinated 2,5-Dimethoxy-2,5-Dihydrofuran for Non-invasive Imaging. ACS Appl. Mater. Interfaces 2014, 6, 17926–17936. [PubMed: 25265599]

(8). Carr TM III; Sabri SS; Turba UC; Park A-W; Saad WEA; Angle JF; Matsumoto AH Stenting for Atherosclerotic Renal Artery Stenosis. Tech Vasc. Interv. Radiol 2010, 13, 134–145. [PubMed: 20540922]

(9). Zhang K; Maier F; Krafft AJ; Umathum R; Semmler W; Bock M Tracking of an Interventional Catheter with a Ferromagnetic Tip Using Dual-echo Projections. J. Magn. Reson 2013, 234, 176–183. [PubMed: 23892103]

(10). Shirato H; Harada T; Harabayashi T; Hida K; Endo H; Kitamura K; Onimaru R; Yamazaki K; Kurauchi N; Shimizu T; Shinohara N; Matsushita M; Dosaka-Akita H; Miyasaka K Feasibility of Insertion/Implantation of 2.0-mm-Diameter Gold Internal Fiducial Markers for Precise Setup and Real-time Tumor Tracking in Radiotherapy. Int. J. Radiat. Oncol., Biol., Phys 2003, 56, 240–247. [PubMed: 12694845]

(11). Cheheltani R; Kim J; Naha P; Cormode DP Nanobiotechnology; Dhawan A, Singh S, Kumar A, Shanker R, Eds.; CRC Press, 2018; pp 219–250.

(12). Lee N; Choi SH; Hyeon T Nano-sized CT Contrast Agents. Adv. Mater 2013, 25, 2641–2660. [PubMed: 23553799]

(13). Saha SK; Oakdale JS; Cuadra JA; Divin C; Ye J; Forien J-B; Bayu Aji L. B.; Biener J; Smith WL Radiopaque Resists for Two-photon Lithography to Enable Submicron 3D Imaging of Polymer Parts via X-ray Computed Tomography. ACS Appl. Mater. Interfaces 2018, 10, 1164–1172. [PubMed: 29171264]

(14). Chandler HH; Bowen RL; Paffenbarger GC Development of a Radiopaque Denture Base Material. J. Biomed. Mater. Res 1971, 5, 253–265. [PubMed: 5561000]

(15). Cook WD An Investigation of the Radiopacity of Composite Restorative Materials. Aust. Dent. J 1981, 26, 105–112. [PubMed: 6941760]

(16). Cabasso I; Smid J; Sahni SK Radiopaque Miscible Systems Composed of Poly(methyl methacrylate) and Transition and Nontransition Metal Salts: Spectroscopic, Thermal, and Radiographic Characterization. J. Appl. Polym. Sci 1989, 38, 1653–1666.

(17). Konduru N; Keller J; Ma-Hock L; Groters S; Landsiedel R; Donaghey TC; Brain JD; Wohlleben W; Molina RM Biokinetics and Effects of Barium Sulfate Nanoparticles. Part. Fibre Toxicol 2014, 11, 55. [PubMed: 25331813]

(18). Horak D; Metalova M; Švec F; Drobnik J; Kalal J; Borovička M; Adamyan A; Voronkova O; Gumargalieva K Hydrogels in Endovascular Embolization. III. Radiopaque Spherical Particles, Their Preparation and Properties. Biomaterials 1987, 8, 142–145. [PubMed: 3580473]

(19). Tamber H; Smid J; Cabasso I Radiopaque Copolymers of Styryldiphenylbismuth Vinylbenzylphosphonate and Methyl Methacrylate. Chem. Mater 1997, 9, 1335–1341.

(20). Cormode DP; Naha PC; Fayad ZA Nanoparticle Contrast Agents for Computed Tomography: a Focus on Micelles. Contrast Media Mol. Imaging 2014, 9, 37–52. [PubMed: 24470293]

(21). Ai K; Liu Y; Liu J; Yuan Q; He Y; Lu L Large-scale Synthesis of Bi2S3 Nanodots as a Contrast Agent for In Vivo X-ray Computed Tomography Imaging. Adv. Mater 2011, 23, 4886–4891. [PubMed: 21956662]

(22). Kinsella JM; Jimenez RE; Karmali PP; Rush AM; Kotamraju VR; Gianneschi NC; Ruoslahti E; Stupack D; Sailor MJ X-ray Computed Tomography Imaging of Breast Cancer by Using Targeted Peptide-labeled Bismuth Sulfide Nanoparticles. Angew. Chem., Int. Ed 2011, 50, 12308–12311.

(23). Cormode DP; Skajaa T; van Schooneveld MM; Koole R; Jarzyna P; Lobatto ME; Calcagno C; Barazza A; Gordon RE; Zanzonico P; Fisher EA; Fayad ZA; Mulder WJM Nanocrystal Core High-Density Lipoproteins: A Multimodality Contrast Agent Platform. Nano Lett 2008, 8, 3715–3723. [PubMed: 18939808]

(24). Jakhmola A; Anton N; Vandamme TF Inorganic Nanoparticles Based Contrast Agents for X-ray Computed Tomography. Adv. Healthcare Mater 2012, 1, 413–431.

(25). Berger M; Bauser M; Frenzel T; Hilger CS; Jost G; Lauria S; Morgenstern B; Neis C; Pietsch H; Sülzle D; Hegetschweiler K Hafnium-Based Contrast Agents for X-ray Computed Tomography. Inorg. Chem 2017, 56, 5757–5761. [PubMed: 28430423]

(26). Davenport MS; Khalatbari S; Cohan RH; Dillman JR; Myles JD; Ellis JH Contrast Material–induced Nephrotoxicity and Intravenous Low-Osmolality Iodinated Contrast Material: Risk Stratification by Using Estimated Glomerular Filtration Rate. Radiology 2013, 268, 719–728. [PubMed: 23579046]

(27). Stacul F; van der Molen AJ; Reimer P; Webb JAW; Thomsen HS; Morcos SK; Almén T; Aspelin P; Bellin MF; Clement O; Heinz-Peer G Contrast Induced Nephropathy Updated ESUR Contrast Media Safety Committee Guidelines. Eur. J. Radiol 2011, 21, 2527–2541.

(28). Allijn IE; Leong W; Tang J; Gianella A; Mieszawska AJ; Fay F; Ma G; Russell S; Callo CB; Gordon RE; Korkmaz E; Post JA; Zhao Y; Gerritsen HC; Thran A; Proksa R; Daerr H; Storm G; Fuster V; Fisher EA; Fayad ZA; Mulder WJM; Cormode DP Gold Nanocrystal Labeling Allows Low-Density Lipoprotein Imaging from the Subcellular to Macroscopic Level. ACS Nano 2013, 7, 9761–9770. [PubMed: 24127782]

(29). Mieszawska AJ; Mulder WJM; Fayad ZA; Cormode DP Multifunctional Gold Nanoparticles for Diagnosis and Therapy of Disease. Mol. Pharmaceutics 2013, 10, 831–847.

(30). Eck W; Nicholson AI; Zentgraf H; Semmler W; Bartling S Anti-CD4-targeted Gold Nanoparticles Induce Specific Contrast Enhancement of Peripheral Lymph Nodes in X-ray Computed Tomography of Live Mice. Nano Lett 2010, 10, 2318–2322. [PubMed: 20496900]

(31). Popovtzer R; Agrawal A; Kotov NA; Popovtzer A; Balter J; Carey TE; Kopelman R Targeted Gold Nanoparticles Enable Molecular CT Imaging of Cancer. Nano Lett 2008, 8, 4593–4596. [PubMed: 19367807]

(32). Galper MW; Saung MT; Fuster V; Roessl E; Thran A; Proksa R; Fayad ZA; Cormode DP Effect of Computed Tomography Scanning Parameters on Gold Nanoparticle and Iodine Contrast. Invest. Radiol 2012, 47, 475–481. [PubMed: 22766909]

(33). Rabin O; Manuel Perez J.; Grimm J; Wojtkiewicz G; Weissleder R An X-ray Computed Tomography Imaging Agent Based on Long-circulating Bismuth Sulphide Nanoparticles. Nat. Mater 2006, 5, 118–122. [PubMed: 16444262]

(34). Naha PC; Al Zaki A; Hecht E; Chorny M; Chhour P; Blankemeyer E; Yates DM; Witschey WRT; Litt HI; Tsourkas A; Cormode DP Dextran Coated Bismuth–iron Oxide Nanohybrid Contrast Agents for Computed Tomography and Magnetic Resonance Imaging. J. Mater. Chem. B 2014, 2, 8239–8248. [PubMed: 25485115]

(35). Brown AL; Naha PC; Benavides-Montes V; Litt HI; Goforth AM; Cormode DP Synthesis, X-ray Opacity, and Biological Compatibility of Ultra-high Payload Elemental Bismuth Nanoparticle X-ray Contrast Agents. Chem. Mater 2014, 26, 2266–2274. [PubMed: 24803727]

(36). Bi H; He F; Dong Y; Yang D; Dai Y; Xu L; Lv R; Gai S; Yang P; Lin J Bismuth Nanoparticles with “Light” Property Served as a Multifunctional Probe for X-ray Computed Tomography and Fluorescence Imaging. Chem. Mater 2018, 30, 3301–3307.

(37). Brown AL; Goforth AM pH-Dependent Synthesis and Stability of Aqueous, Elemental Bismuth Glyconanoparticle Colloids: Potentially Biocompatible X-ray Contrast Agents. Chem. Mater 2012, 24, 1599–1605.

(38). Song G; Liang C; Gong H; Li M; Zheng X; Cheng L; Yang K; Jiang X; Liu Z Core–Shell MnSe@Bi2Se3 Fabricated via a Cation Exchange Method as Novel Nanotheranostics for Multimodal Imaging and Synergistic Thermoradiotherapy. Adv. Mater 2015, 27, 6110–6117. [PubMed: 26331476]

(39). Pan D; Roessl E; Schlomka JP; Caruthers SD; Senpan A; Scott MJ; Allen JS; Zhang H; Hu G; Gaffney PJ; Choi ET; Rasche V; Wickline SA; Proksa R; Lanza GM Computed Tomography in Color: NanoK-Enhanced Spectral CT Molecular Imaging. Angew. Chem., Int. Ed 2010, 49, 9635–9639.

(40). Swy ER; Schwartz-Duval AS; Shuboni DD; Latourette MT; Mallet CL; Parys M; Cormode DP; Shapiro EM Dual-modality, Fluorescent, PLGA Encapsulated Bismuth Nanoparticles for Molecular and Cellular Fluorescence Imaging and Computed Tomography. Nanoscale 2014, 6, 13104–13112. [PubMed: 25248645]

(41). Yang S; Li Z; Wang Y; Fan X; Miao Z; Hu Y; Li Z; Sun Y; Besenbacher F; Yu M Multifunctional Bi@PPy-PEG Core–Shell Nanohybrids for Dual-modal Imaging and Photothermal Therapy. ACS Appl. Mater. Interfaces 2018, 10, 1605–1615. [PubMed: 29272573]

(42). Wei B; Zhang X; Zhang C; Jiang Y; Fu YY; Yu C; Sun SK; Yan XP Facile Synthesis of Uniform-sized Bismuth Nanoparticles for CT Visualization of Gastrointestinal Tract in Vivo. ACS Appl. Mater. Interfaces 2016, 8, 12720–12726

(43). Deng J; Xu S; Hu W; Xun X; Zheng L; Su M Tumor Targeted, Stealthy and Degradable Bismuth Nanoparticles for Enhanced X-ray Radiation Therapy of Breast Cancer. Biomaterials 2018, 154, 24–33. [PubMed: 29120816]

(44). Li Z; Liu J; Hu Y; Li Z; Fan X; Sun Y; Besenbacher F; Chen C; Yu M Biocompatible PEGylated Bismuth Nanocrystals: “All-in-one” Theranostic Agent with Triple-modal Imaging and Efficient in vivo Photothermal Ablation of Tumors. Biomaterials 2017, 141, 284–295. [PubMed: 28709019]

(45). Hernández-Rivera M; Kumar I; Cho SY; Cheong BY; Pulikkathara MX; Moghaddam SE; Whitmire KH; Wilson LJ High-performance Hybrid Bismuth–Carbon Nanotube Based Contrast Agent for X-ray CT Imaging. ACS Appl. Mater. Interfaces 2017, 9, 5709–5716.

(46). Briand GG; Burford N Bismuth Compounds and Preparations with Biological or Medicinal Relevance. Chem. Rev 1999, 99, 2601–2658. [PubMed: 11749495]

(47). Shukla R; Bansal V; Chaudhary M; Basu A; Bhonde RR; Sastry M Biocompatibility of Gold Nanoparticles and Their Endocytotic Fate Inside the Cellular Compartment: A Microscopic Overview. Langmuir 2005, 21, 10644–10654. [PubMed: 16262332]

(48). Mjos KD; Orvig C Metallodrugs in Medicinal Inorganic Chemistry. Chem. Rev 2014, 114, 4540–4563. [PubMed: 24456146]

(49). Daniel MC; Astruc D Gold Nanoparticles: Assembly, Supramolecular Chemistry, Quantum-size-related Properties, and Applications toward Biology, Catalysis, and Nanotechnology. Chem. Rev 2004, 104, 293–346. [PubMed: 14719978]

(50). Hostetler MJ; Green SJ; Stokes JJ; Murray RW Monolayers in Three Dimensions: Synthesis and Electrochemistry of ω-Functionalized Alkanethiolate-Stabilized Gold Cluster Compounds. J. Am. Chem. Soc 1996, 118, 4212–4213.

(51). Li N; Zhao P; Astruc D Anisotropic Gold Nanoparticles: Synthesis, Properties, Applications, and Toxicity. Angew. Chem., Int. Ed 2014, 53, 1756–1789.

(52). Soo Choi H; Liu W; Misra P; Tanaka E; Zimmer JP; Itty Ipe B.; Bawendi MG; Frangioni JV Renal Clearance of Quantum Dots. Nat. Biotechnol 2007, 25, 1165–1170. [PubMed: 17891134]

(53). Sun H; Li H; Harvey I; Sadler PJ Interactions of Bismuth Complexes with Metallothionein(II). J. Biol. Chem 1999, 274, 29094–29101. [PubMed: 10506163]

(54). Wang Y; Zhao J; Zhao X; Tang L; Li Y; Wang Z A Facile Water-based Process for Preparation of Stabilized Bi Nanoparticles. Mater. Res. Bull 2009, 44, 220–223.

(55). Zhang G; Chan JMW Reversibly Thermochromic Bismuth-Organic Materials with Tunable Optical Gaps. J. Mater. Chem. C 2017, 5, 10007–10015.

(56). Gilman H; Yale HL Preferential Cleavage of Radicals in Organobismuth and Organomercury Compounds. J. Am. Chem. Soc 1950, 72, 8–10.

(57). Gilman H.; Nelson JF. Relative Reactivities of Organometallic Compounds. XVI. Detection of the —SH Group. J. Am. Chem. Soc 1937, 59, 935–937.

(58). Luqman A; Blair VL; Bond AM; Andrews PC Formation of Bismuth(V) Thiolates: Protolysis and Oxidation of Triphenylbismuth(III) with Heterocyclic Thiols. Angew. Chem., Int. Ed 2013, 52, 7247–7251.

(59). Huston P; Espenson JH; Bakac A Reactions of Thiyl Radicals with Transition-metal Complexes. J. Am. Chem. Soc 1992, 114, 9510–9516.

(60). Farrugia LJ; Lawlor FJ; Norman NC Bismuth(III) Thiolates: Syntheses and the Structures of a Neutral Thiolate and a Thiolato Anion. Polyhedron 1995, 14, 311–314.

(61). Anderson KM; Baylies CJ; Monowar Jahan A. H. M.; Norman NC; Orpen AG; Starbuck J Coordination Complexes of the Bismuth(III) Thiolates Bi(SC6F5)3 and Bi(SC6Cl5)3 with Pyridine Ligands. Dalton Trans 2003, 0, 3270–3277.

(62). Gilman H.; Yale HL. The Products of the Cleavage of Triarylbismuth Derivatives by SH-Containing Compounds. J. Am. Chem. Soc 1951, 73, 2880–2881.

(63). Kennedy BP; Lever ABP Studies of the Metal–Sulfur Bond. Complexes of the Pyridine Thiols. Can. J. Chem 1972, 50, 3488–3507.

(64). Petrov AI; Golovnev NN; Dergachev ID; Leshok AA Complex Formation of Bismuth(III) with 2-Mercaptoethanesulfonic and 3-Mercaptopropanesulfonic Acids: Experimental and Theoretical Study. Polyhedron 2013, 50, 59–65.

(65). Petrov AI; Dergachev ID; Trubina SV; Erenburg SB; Lutoshkin MA; Golovnev NN; Kondrasenko AA; Dergachev VD Complexation of Bi(III) with 3-Mercaptopropionic Acid in Aqueous Solutions: a Combined Experimental and Theoretical Study. RSC Adv 2014, 4, 52384–52392.

(66). Zumeta-Dubé I; Ortiz-Quiñonez J-L; Díaz D; Trallero-Giner C; Ruiz-Ruiz V-F First Order Raman Scattering in Bulk Bi2S3 and Quantum Dots: Reconsidering Controversial Interpretations. J. Phys. Chem. C 2014, 118, 30244–30252.

(67). Kaltenhauser V; Rath T; Haas W; Torvisco A; Müller SK; Friedel B; Kunert B; Saf R; Hofer F; Trimmel G Bismuth Sulphide–Polymer Nanocomposites from a Highly Soluble Bismuth Xanthate Precursor. J. Mater. Chem. C 2013, 1, 7825–7832.

(68). Trentelman K A Note on the Characterization of Bismuth Black by Raman Microspectroscopy. J. Raman Spectrosc 2009, 40, 585–589.

(69). Naha PC; Lau KC; Hsu JC; Hajfathalian M; Mian S; Chhour P; Uppuluri L; McDonald ES; Maidment ADA; Cormode DP Gold Silver Alloy Nanoparticles (GSAN): an Imaging Probe for Breast Cancer Screening with Dual-energy Mammography or Computed Tomography. Nanoscale 2016, 8, 13740–13754. [PubMed: 27412458]

(70). Malfertheiner P; Bazzoli F; Delchier J-C; Celiński K; Giguère M; Rivière M; Mégraud F Helicobacter pylori Eradication with a Capsule Containing Bismuth Subcitrate Potassium, Metronidazole, and Tetracycline Given with Omeprazole versus Clarithromycin-based Triple

Therapy: a Randomised, Open-label, Non-inferiority, Phase 3 Trial. Lancet 2011, 377, 905–913. [PubMed: 21345487]

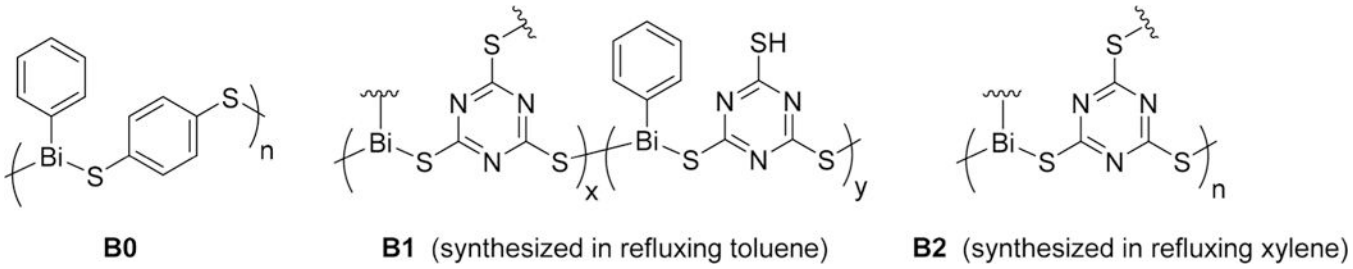

Figure 1.

Structures of three bismuth-containing coordination polymers **B0, B1**, and **B2**, as synthesized by polycondensations between triphenylbismuth and a dithiol or trithiol.

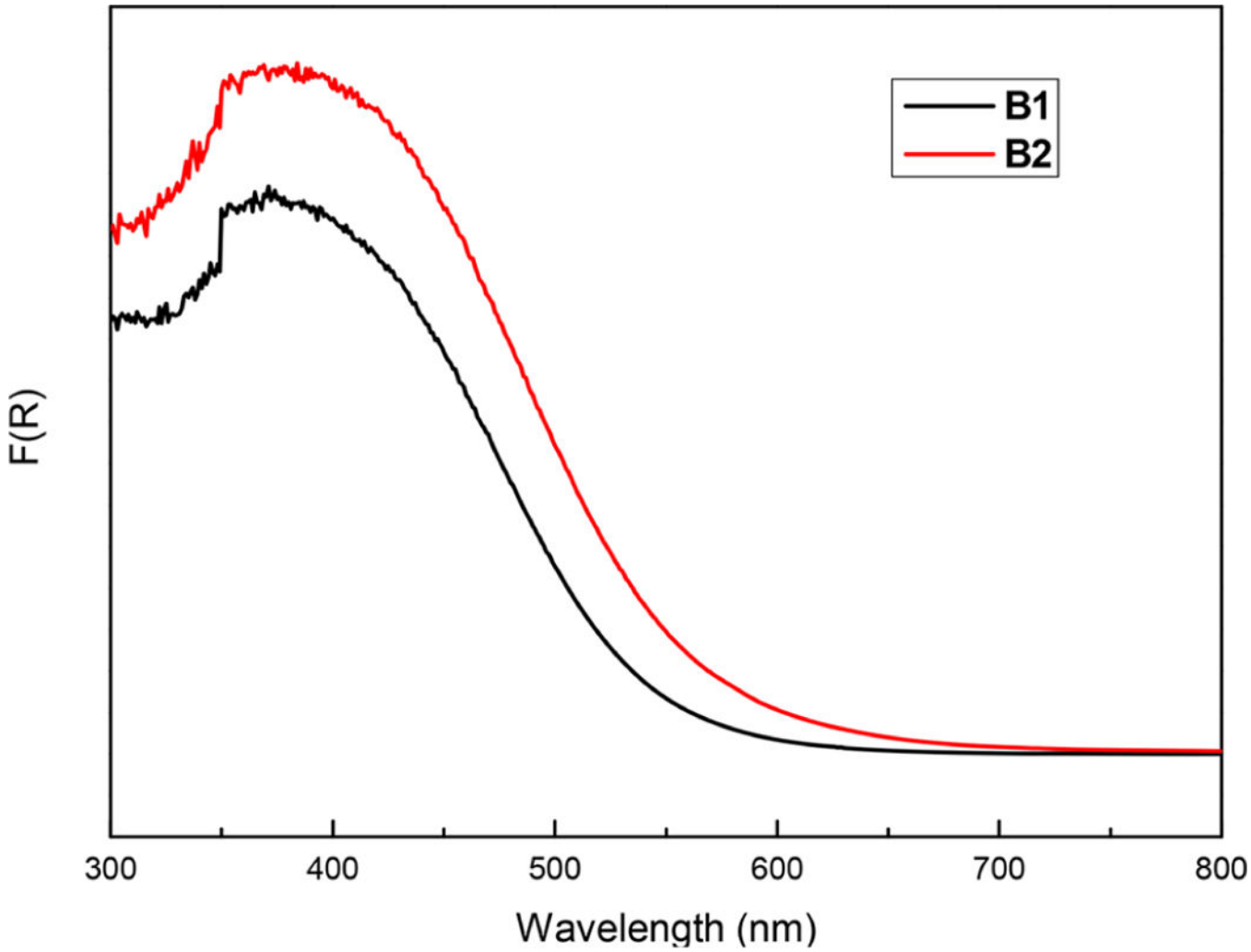

Figure 2.
Solid-state UV–vis diffuse reflectance spectra of polymers **B1** and **B2.**

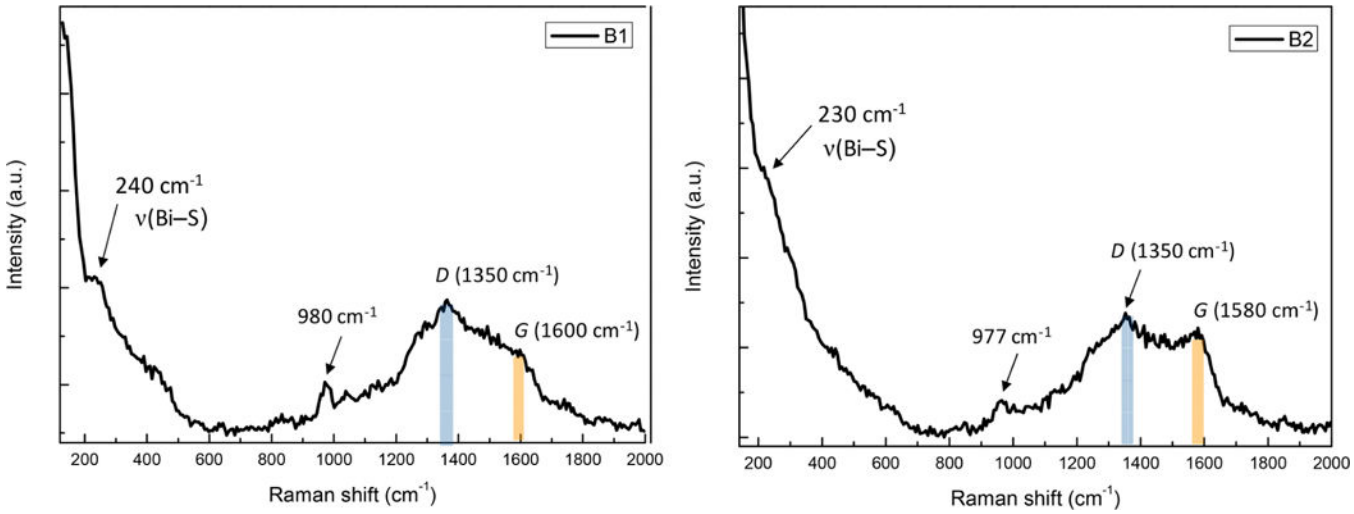

Figure 3.
Raman spectra of polymers **B1** and **B2**, showing the characteristic structural features.

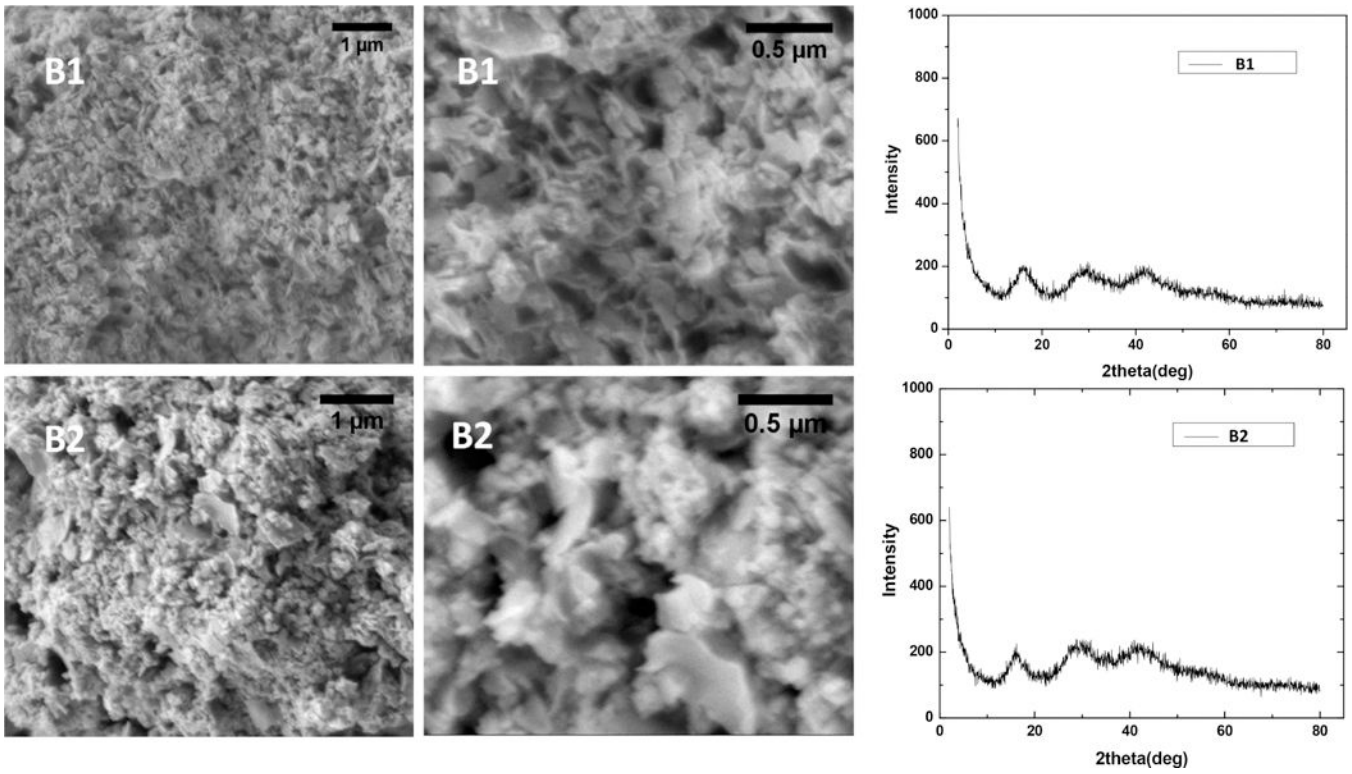

Figure 4.
SEM images and PXRD patterns of **B1** and **B2.**

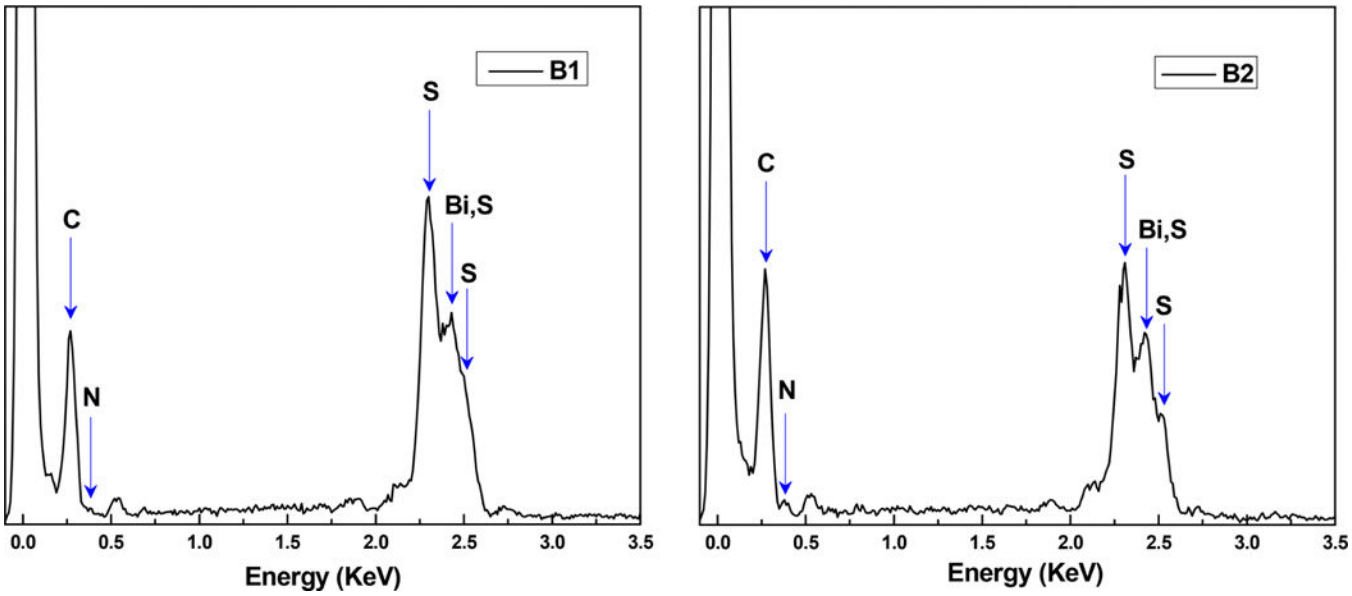

Figure 5.
EDS spectra of **B1** and **B2** showing their elemental compositions.

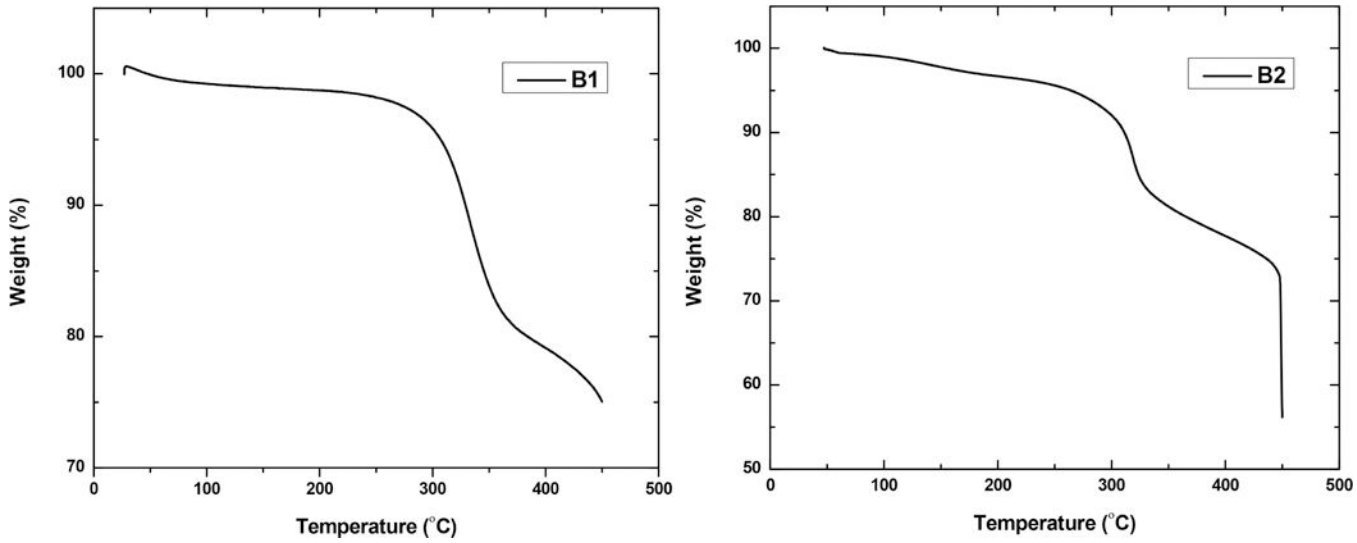

Figure 6.
TGA curves of polymers **B1** and **B2**.

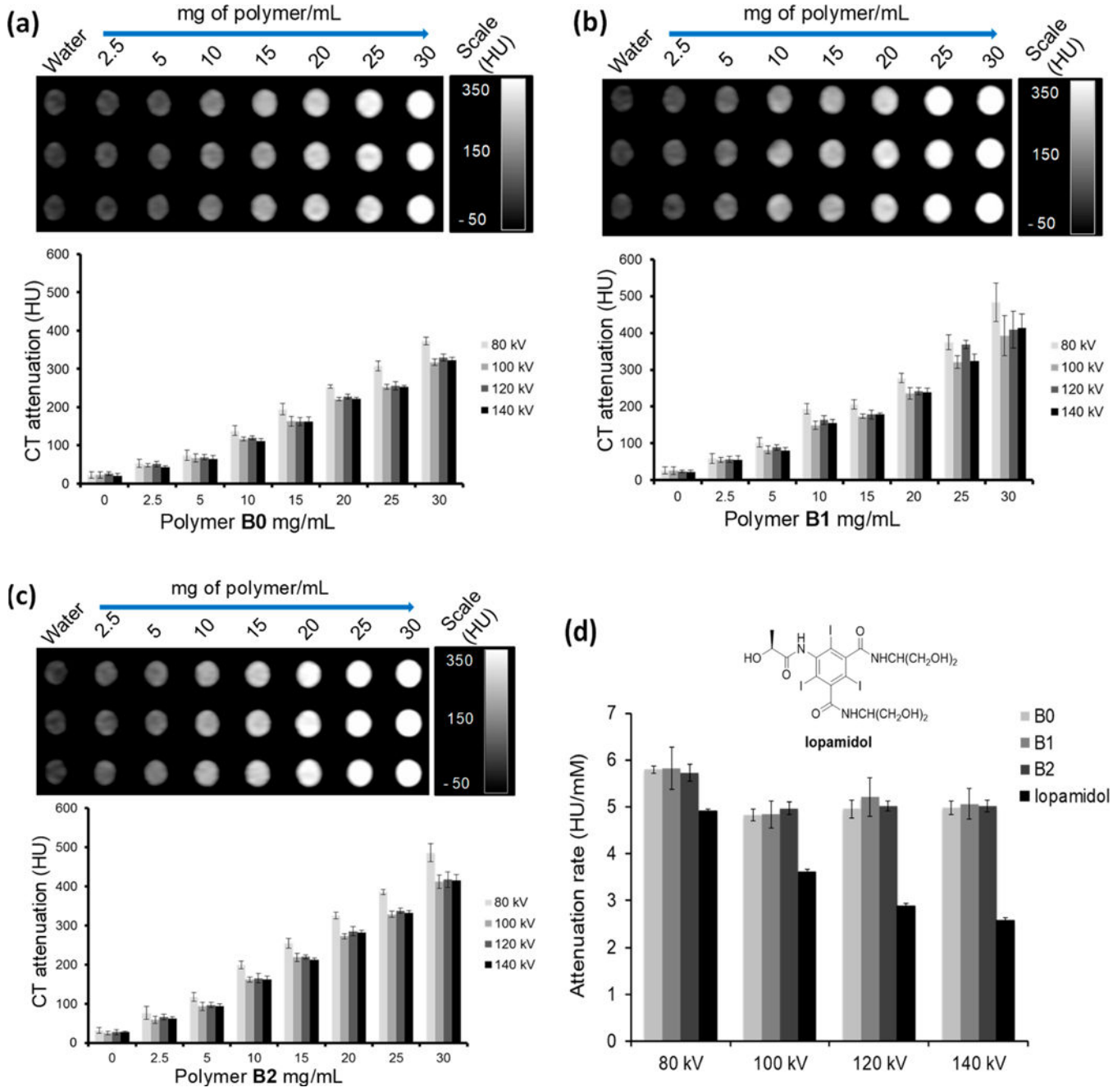

Figure 7.

CT attenuation evaluation of **B0, B1**, and **B2:** (a) CT image (at 80 kV) of polymer **B0** dispersions at concentrations ranging from 2.5 to 30 mg/mL, and a plot showing CT attenuation (HU) vs polymer concentration; (b) CT image and plot for **B1** dispersions at the same tube voltage and concentration range; (c) CT image and plot for **B2** (same parameters as above); (d) CT contrast properties of polymers **B0, B1**, and **B2** vs Iopamidol.

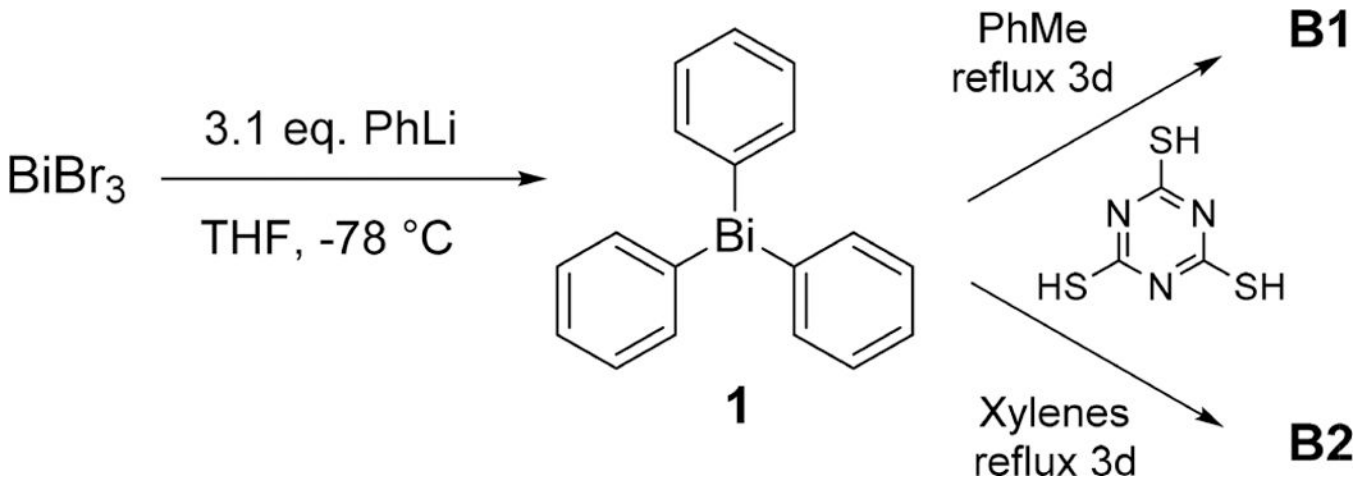

Scheme 1.
Synthesis of Bismuth Thiolate Coordination Polymers B1 and B2